JACS
JOURNAL OF THE AMERICAN CHEMICAL SOCIETY
Article
pubs.acs.org/JACS

Enabling Light Work in Helical Self-Assembly for Dynamic Amplification of Chirality with Photoreversibility

Yunsong Cai,[†,§] Zhiqian Guo,[†,§] Jianmei Chen,[‡] Wenlong Li,[†] Liubiao Zhong,[‡] Ya Gao,[∥] Lin Jiang,[‡] Lifeng Chi,[*,‡,⊥] He Tian,[†] and Wei-Hong Zhu[*,†]

[†]Key Laboratory for Advanced Materials and Institute of Fine Chemicals, Shanghai Key Laboratory of Functional Materials Chemistry, East China University of Science and Technology, Shanghai 200237, P. R. China

[‡]Institute of Functional Nano & Soft Materials (FUNSOM), Soochow University, Suzhou 215123, P. R. China

[⊥]Physikalisches Institut and Center for Nanotechnology (CeNTech), Universität Münster, Münster 48149, Germany

[∥]College of Fundamental Studies, Shanghai University of Engineering Science, Shanghai 201620, P. R. China

Supporting Information

ABSTRACT: Light-driven transcription and replication are always subordinate to a delicate chirality transfer. Enabling light work in construction of the helical self-assembly with reversible chiral transformation becomes attractive. Herein we demonstrate that a helical hydrogen-bonded self-assembly is reversibly photoswitched between photochromic open and closed forms upon irradiation with alternative UV and visible light, in which molecular chirality is amplified with the formation of helixes at supramolecular level. The characteristics in these superhelixes such as left-handed or right-handed twist and helical length, height, and pitch are revealed by SEM and AFM. The helical photoswitchable nanostructure provides an easily accessible route to an unprecedented photoreversible modulation in morphology, fluorescence, and helicity, with precise assembly/disassembly architectures similar to biological systems such as protein and DNA.

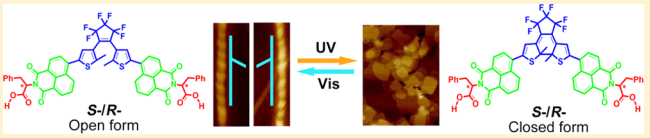

INTRODUCTION

Self-assembly architecture of helical nanostructures is of great interest because of its potential insight into biological systems and material science. Nanoscience and nanotechnology have been logically merged, along with moving hand in hand via academic and industrial endeavors.[1−7] There have been established several strategies to artificial helixes, such as hydrogen-bonding,[8,9] $\pi-\pi$ stacking,[10−12] template method,[13] "majority-rules" and "sergeants-soldiers" principle,[14] in gelation state[15] or liquid crystal media.[16,17] Particularly, perylene bisimides[18,19] and naphthalene diimides[20,21] are exploited as fluorescent building blocks in construction of these thermodynamically helical nanostructures. Photochromic diarylethenes (DAEs) have also attracted much attention since their chemical and physical properties are reversibly controllable with photoirradiation,[22−24] especially for their functional switching characteristics,[25−31] such as the photoresponsive helical gel[13,32] and light-driven self-assembly.[33,34] However, the dynamic photoreversibility with modulation of amplified chirality and morphology as well as fluorescence between two thermally stable states are still remaining challenges.

Here we intend to construct a unique supramolecular helical architecture with combining three functional units (Figure 1a): (i) the chirality in common α-amino acids, such as two enantiomers of (*S*-/*R*-) phenylalanine, for hydrogen-bond-induced helical self-assembly, (ii) naphthalimide chromophore[35,36] for fluorescence modulation by photoswitching, and (iii) bistable photoresponsive DAE for dynamic photoswitching. With respect to the precursor ester ***S*-2**$_o$ and the butyl derivative **3** as reference (Figure 1a), the DAE-embedded ***S*-/*R*-1**$_o$ can realize a thermodynamic amplification of helical chirality in the process of self-assembly. Interestingly, using the α-chiral carboxylic acid dimer as the helicity generator, the specific one-dimensional left-/right-handed helixes are exactly dependent upon the chirality in amino acids of (*S*-/*R*-) phenylalanine in the triad system. As demonstrated, the helical nanostructure undergoes a reversible fluorescence on−off and assembly−disassembly process upon irradiation of supramolecular solution with alternative UV and visible light. Moreover, the fascinating photoswitchable chiral amplification from helical self-assembly can serve as a great breakthrough to chiral communication between molecular and supramolecular chirality.

RESULTS AND DISCUSSION

Synthesis. The target building blocks ***S*-/*R*-1**$_o$ were synthesized by hydrolysis from their reference compounds ***S*-/*R*-2**$_o$, which were obtained by Suzuki cross-coupling reaction of naphthalimide borate and dibromo-substituted DAEs (Scheme S1 in Supporting Information, SI). Meanwhile the butyl derivative **3** was also prepared as reference compound. The detailed procedure is described in the SI. All the compounds were characterized by ^{1}H and ^{13}C NMR spectra as well as HRMS spectra.

Received: November 5, 2015
Published: December 28, 2015

DOI: 10.1021/jacs.5b11580
J. Am. Chem. Soc. 2016, 138, 2219−2224

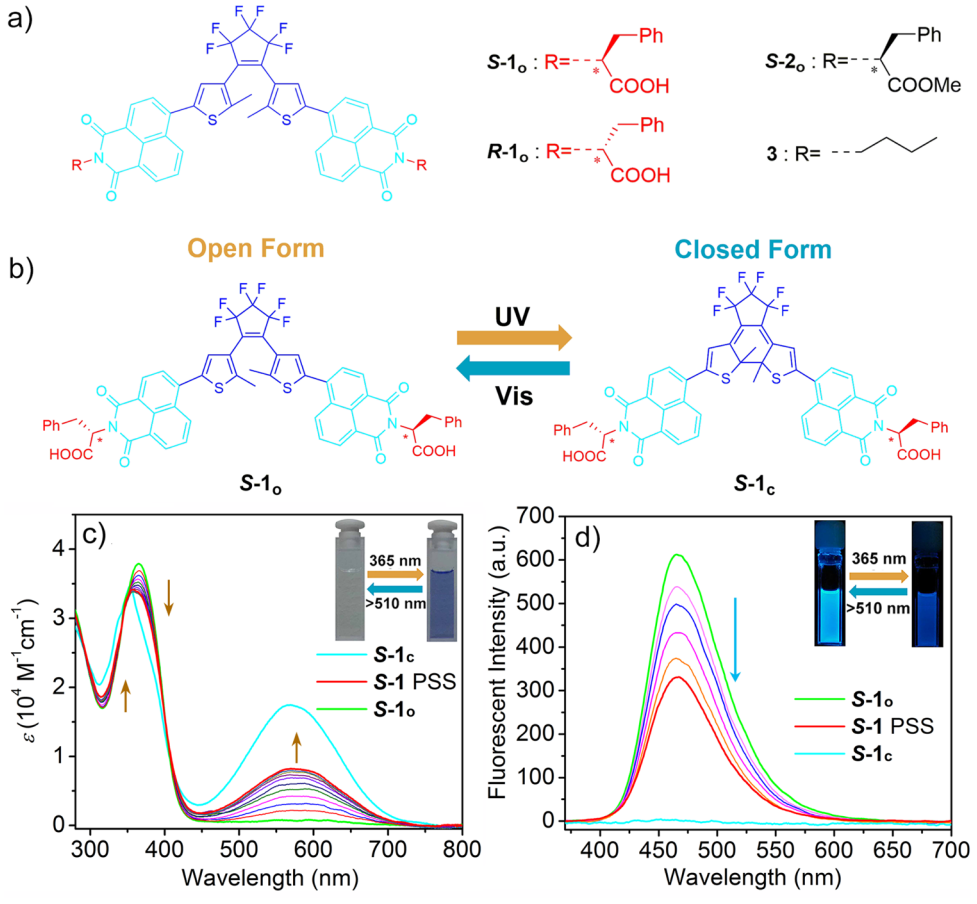

Figure 1. Photochromic behavior and fluorescent regulation: (a) Molecular structures of building blocks ***S*-1$_o$** and ***R*-1$_o$**, and reference compounds ***S*-2$_o$** and **3**. Note: "*R*" and "*S*" represents the chirality of amino acids, subscripts "o" and "c" describe the corresponding open and closed forms, respectively, and ***S*-1** PSS is defined as the photostationary state of isomerization of ***S*-1$_o$**. For ***S*-1$_o$** or ***S*-2$_o$**, its chiral amino acid has a "***S***" configuration and "***R***" configuration for ***R*-1$_o$**. (b) Photoisomerization of ***S*-1$_o$**. Irradiation with 365 nm in CCl_4 at 25 °C ($c = 2 \times 10^{-5}$ M): (c) absorption changes of ***S*-1$_o$** (interval: 60 s) and ***S*-1$_c$**, and (d) fluorescence changes of ***S*-1$_o$** excited at 365 nm.

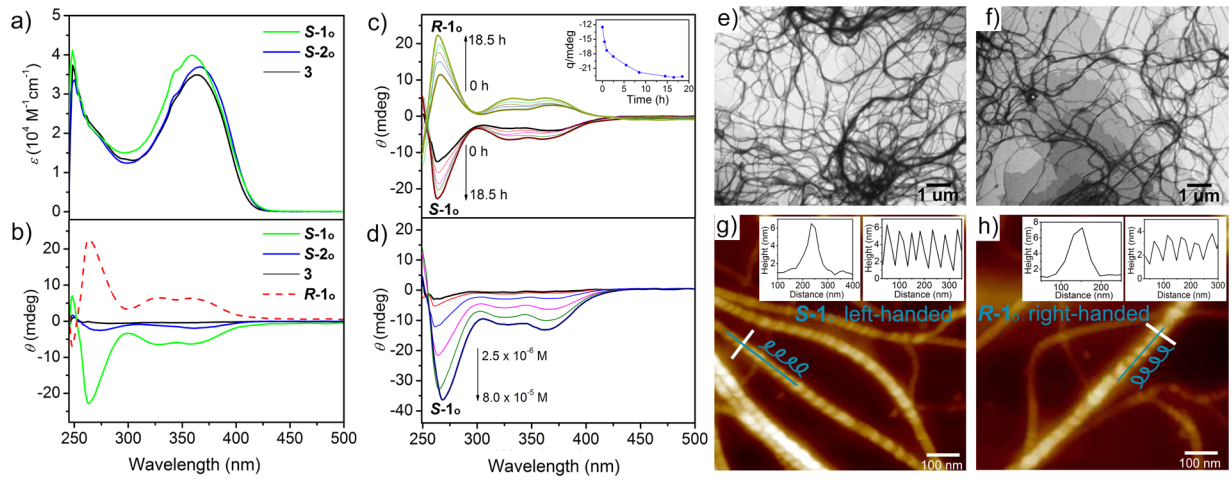

Figure 2. CD amplification in CCl_4 at 25 °C and morphology observation of helical self-assembly: (a) Absorbance spectra of ***S*-1$_o$**, ***S*-2$_o$** and **3** ($c = 2 \times 10^{-5}$ M). (b) CD spectra of ***S*-1$_o$**, ***R*-1$_o$**, ***S*-2$_o$**, and **3** ($c = 2 \times 10^{-5}$ M), measured after aging for 24 h, ensuring its completion of self-assembly. (c) Time-dependent CD spectra of ***S*-1$_o$** and ***R*-1$_o$** ($c = 2 \times 10^{-5}$ M, insert: the growth tendency of ellipticity value at 267 nm of ***S*-1$_o$** with increasing time, 0–18.5 refers to incubation upon dissolution). (d) CD spectral changes of ***S*-1$_o$** at various concentrations (2.5×10^{-6}, 5.0×10^{-6}, 1.0×10^{-5}, 2×10^{-5}, 4×10^{-5}, and 8×10^{-5} M). (e and f) SEM images of ***S*-1$_o$** and ***R*-1$_o$**, respectively. (g and h) AFM images of ***S*-1$_o$** and ***R*-1$_o$** (insert: cross sectional analysis of height along white line and helical pitch along blue line).

Photoswitching Behavior and Fluorescent Regulation. As illustrated in Figure 1b, the photoswitching behavior of the open DAE ***S*-1$_o$** containing (*S*)-phenylalanine was first studied. Irradiation of a CCl_4 solution of ***S*-1$_o$** with 365 nm resulted in the characteristic ring-closing reaction of ***S*-1$_o$** to give ***S*-1$_c$**.[22] During the photochromic process (Figure 1c), the colorless solution of

DOI: 10.1021/jacs.5b11580
J. Am. Chem. Soc. 2016, 138, 2219–2224

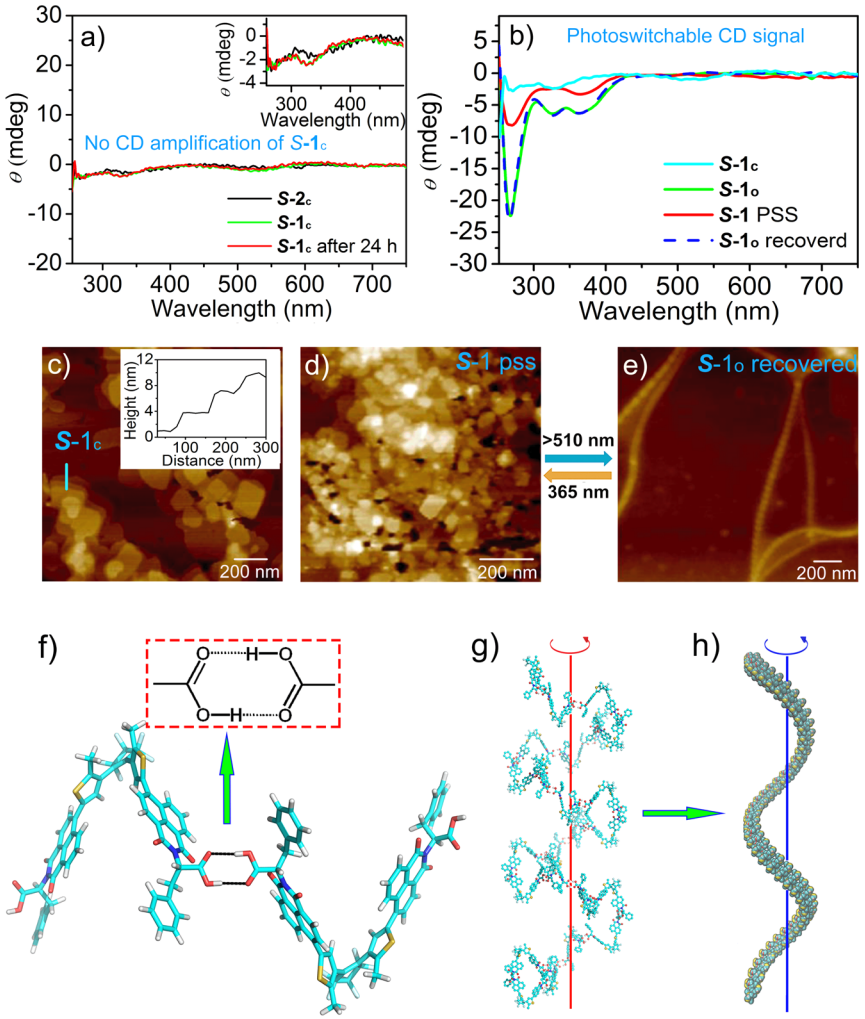

Figure 3. Nonhelical aggregation of ***S*-1$_c$** and photoreversible helicity control: (a) CD spectra of ***S*-2$_c$**, ***S*-1$_c$** (tested immediately), and ***S*-1$_c$** (tested after aging for 24 h). (b) CD spectra of ***S*-1$_c$**, ***S*-1$_o$**, ***S*-1** PSS (irradiation with 365 nm), ***S*-1$_o$** recovered (irradiation of PSS solution with visible light, $\lambda > 510$ nm, measured after aging for 24 h), $c = 2 \times 10^{-5}$ M in CCl_4 at 25 °C. AFM images: (c) ***S*-1$_c$** (tested after aging for 24 h), insert: cross section analysis of height along blue line, (d) ***S*-1** PSS and (e) ***S*-1$_o$** recovered. Molecular model of helical nanostructures: (f) extraction of repeating unit: intermolecular hydrogen bonding between neighboring ***S*-1$_o$** (length of hydrogen bond: 2.1 Å), (g) side view of energy-optimized primary helix self-assembled from ***S*-1$_o$** (left-handed, red line: axis of primary helix), (h) computer-generated representation of secondary helix (blue line: axis of secondary helix). Note: the left-handed primary helix relaxes into a left-handed secondary helix, but the height and pitch of secondary helix are larger than primary helix.

***S*-1$_o$** turned blue and eventually reached photostationary state (PSS) accompanied by an increase of new absorption band in the range of 430−710 nm (λ_{max} = 588 nm) and a decrease of absorption band at 352 nm. Due to the same embedded DAE unit of ***S*-1$_o$**, reference compounds ***S*-2$_o$** and **3** showed the similar photochromic behaviors (Figure S1 in SI). Notably, the closed isomer ***S*-1$_c$**, exhibiting the highly thermal stability, was successfully separated with preparative chromatography. Upon irradiation with visible light ($\lambda > 510$ nm), the resulting ***S*-1$_c$** was completely turned back to ***S*-1$_o$**. The reversible photoisomerization could be repeated many times without remarkable degradation (Figure S2a in SI). Interestingly, upon transforming the ester group into carboxylic acid, the conversion ratio (CR) from ***S*-1$_o$** to ***S*-1$_c$** (48.3%) became much lower than that of ***S*-2$_o$** (83.5%, Table S1 in SI). It may arise from the high cycloreversion quantum yield from ***S*-1$_c$** to ***S*-1$_o$** (13.6%) with respect to that of ***S*-2$_c$** to ***S*-2$_o$** (2.3%).

As shown in Figure 1d, open isomer ***S*-1$_o$** shows noticeable fluorescence at 470 nm, which can be readily modulated by photochromic reaction. Indeed, no fluorescent signal from naphthalimide moiety[35,36] was detected from the pure closed form ***S*-1$_c$**. The PSS solution resulting from pure open form ***S*-1$_o$** demonstrated a significant fluorescence quenching by 46%, consistent with photocyclization yield at PSS (48%). Accordingly, the fluorescence quenching can be mainly attributed to the formation of nonfluorescent ***S*-1$_c$**. Reference compounds ***S*-2$_o$** and **3** also showed similar properties as ***S*-1$_o$**. The characteristic photoisomerization was also well confirmed by ^{1}H NMR (Figure S3 in SI).

Hydrogen-Bonded Helical Self-Assembly of *S*-1$_o$. The circular dichroism (CD) spectroscopy is indispensable for interpreting chirality of supramolecular self-assembly.[37,38] Figure 2b shows the CD spectra of ***S*-1$_o$**, ***R*-1$_o$**, ***S*-2$_o$**, and **3** ($c = 2 \times 10^{-5}$ M) in nonpolar solvent CCl_4. To ensure the completion of self-assembly, all the samples were tested after aging for 24 h. As expected, reference compound **3** is CD silent, showing no peaks owing to the absence of chiral amino acid group. In contrast, ***S*-1$_o$** and ***R*-1$_o$** exhibited two exact mirror and sharp CD signals with substantial characteristic Cotton effects (CEs). For instance, a positive CE peak at 247 nm and negative CE peaks at 267, 324,

DOI: 10.1021/jacs.5b11580
J. Am. Chem. Soc. 2016, 138, 2219−2224

and 363 nm were observed in the CD curve of ***S*-1$_o$**, and the bisignate exciton couplet with zero crossing at 253 nm and strong nonbisignate CE at 324 and 363 nm corresponded to the absorption region of 250−430 nm (Figure 2a). Notably, the corresponding reference ester ***S*-2$_o$** showed much weaker CD signal response despite that ***S*-2$_o$** bestowed a similar molar extinction coefficient with ***S*-1$_o$**. Upon changing from the ester group (***S*-2$_o$**) to the carboxylic group (***S*-1$_o$**), the approximate 8-fold enhancement in CD signal of ***S*-1$_o$** was observed. Obviously, we can rule out that the CD amplification is from the asymmetric carbon center. Here the CD amplification is critically dependent upon the existence of carboxylic group, which is expected due to the formation of helical supramolecules via intermolecular hydrogen bonding between neighboring carboxylic groups.[39] The CD curves of ***S*-1$_o$** plunged remarkably and approximately reached the same level of reference ester ***S*-2$_o$** upon adding methanol as a breaking agent of hydrogen bonds (16%, v/v, Figure S4a in SI). The decrease in CD signals can be attributed to the rupture of the intermolecular hydrogen bonds, resulting in the disassembly of helical supramolecular structures. Apparently, ***S*-1$_o$** is expected to spontaneously construct helical self-assembly through the intermolecular hydrogen bonding. In addition, ***S*-1$_o$** and ***R*-1$_o$** containing enantiotopic amino acid residues express exactly opposite CD behaviors, indicative of the formation of two enantiotopic helixes.[20] The helical senses of these nanostructures are derived from the bisignate signals at 245−300 nm in their CD spectra, from which we deduce that ***S*-1$_o$** possessing a positive couplet is left-handed, and ***R*-1$_o$** is right-handed with a negative couplet.[16,21,40,41]

For further insight into the kinetics of the CD enhancement, we investigated the time-dependent CD spectral changes of ***S*-1$_o$** and ***R*-1$_o$** (Figure 2c). The absolute ellipticity values at 267, 324, and 363 nm increased significantly with aging time and leveled off after approximately 18.5 h, indicating that the self-assembly based on intermolecular hydrogen bonding is a time-dependent dynamic process. It is noteworthy that the value rose rapidly at the initial period with respect to the last hours. The CD curve is matchable with an isodesmic plot, suggestive of the self-assembly process via isodesmic mechanism.[20,42,43] Moreover, nearly 12-fold enhancement in CD intensity was observed when increasing concentration from 2.5×10^{-6} to 8×10^{-5} M (Figure 2d). For reference compound ***S*-2$_o$**, the CD signals remained the same with extending time even after 48 h (Figure S4d in SI). This time-dependent chiral amplification strongly manifests the dynamic formation of helical supramolecules during the self-assembly.

Fortunately, the morphology of chiral helixes can be directly observed with scanning electron microscope (SEM) and atomic force microscope (AFM). SEM images revealed that ***S*-1$_o$** and ***R*-1$_o$** indeed self-assembled into a well-defined fibrous network with the length approaching micrometer scale (Figure 2g,f). Nevertheless, references ***S*-2$_o$** and **3** show amorphous particles rather than nanofibers (Figure S5 in SI). Fortunately, AFM examination provided us with more precise evidence of these helical nanostructures (Figure 2f,h). A well-defined helical morphology was visualized with a height of approximately 6 nm and a helical pitch of around 50 nm, which were conformationally uniform in size and shape. As discussed above, the opposite CD signals of ***S*-1$_o$** and ***R*-1$_o$** illustrate that the helical sense of nanostructures is biased owing to the incorporation of (*S*-/*R*-) chiral amino acid residues, respectively. From the AFM images, the supramolecular assembly derived from ***S*-1$_o$** has a left-handed (*M*-type) conformational helix, and conversely ***R*-1$_o$** is right-handed (*P*-type). Here the interconnected nanofibers with apparent helix can directly demonstrate that the chiral amplification stems from the hydrogen-bonded helical self-assembly, and the terminal chiral amino-acid moieties can exactly induce the supramolecular chiral nanohelixes.

Nonhelical Aggregation of *S*-1$_c$. As discussed above, the open isomer ***S*-1$_o$** can form helixes in CCl_4 and expresses a dynamic CD amplification. The same experiment was carried out on pure ***S*-1$_c$** to identify whether the closed form ***S*-1$_c$** could self-assemble into helical nanostructures or not. Unexpectedly, the CD signal of ***S*-1$_c$** is as weak as that of the reference ester ***S*-2$_c$** and showed no CD amplification with aging time (Figure 3a), indicating that the closed form ***S*-1$_c$** is not able to spontaneously self-assemble into the similar nanostructures like the corresponding open form ***S*-1$_o$**, that is, no formation of helical structures for ***S*-1$_c$**. AFM further revealed that ***S*-1$_c$** aggregated into lamellar granules with height approximately 4 nm (Figure 3c). Hence the aggregation of ***S*-1$_c$** does have any helical property, along without any CD or chiral amplification. Compared with the open form ***S*-1$_o$**, the closed form ***S*-1$_c$** bestows more planarity and rigidity in molecular conformation, which might lack the flexibility of helical self-assembly.

Making Light Work in Photoswitchable Self-Assembly and Disassembly. Next, we focused on the photoswitchable modulation in these helixes during the photoresponsive behavior between the open and closed forms. As mentioned above, upon irradiation of ***S*-1$_o$** in CCl_4 at 365 nm, the photocyclized ***S*-1$_c$** formed and reached a PSS in colored solution. Meanwhile, the CD signal decreased remarkably along with the photocyclization (Figure 3b). Since the corresponding ester ***S*-2$_o$** does not have the ability of helical self-assembly, its corresponding CD signal shows no response to light stimuli (Figure S4d in SI). AFM images revealed that the photoisomerization from ***S*-1$_o$** to ***S*-1$_c$** at PSS resulted in a dramatic morphology change: The helical nanofibers of open isomer ***S*-1$_o$** were fragmented into amorphous particles (Figure 3d). Due to the relative low conversion ratio from ***S*-1$_o$** to ***S*-1$_c$**, the CD signal of ***S*-1** at PSS was still stronger than pure ***S*-1$_c$**, but the specific helical nanofibers were hardly observed in AFM image. Obviously, both the CD signals and AFM images indicate that, due to the structural rigidity of ***S*-1$_c$**, the segmentally conformational change may bring vital effects on the dynamic stabilization of flexible helixes, that is, disassembling the well-ordered hydrogen-bond permutation.

Photoreversibility is a very important feature for photochromic DAEs. Here colorless ***S*-1$_o$** was recovered completely by irradiation of ***S*-1$_c$** with visible light (λ > 510 nm). Most importantly, in Figure 3b, the CD signals were recovered to the same level of ***S*-1$_o$** (tested after aging for 24 h), indicative of the reassembly of original helical nanostructures. Also from the AFM image of recovered ***S*-1$_o$** (Figure 3e), we observed the same helical nanostructures as the initial solution of ***S*-1$_o$**. In this case, the photoreversible CD change between open form and PSS was able to repeat several times upon irradiation of supramolecular solution with alternative UV and visible light (Figure S2b in SI).

The open form of DAE contains two interchangeable conformations (Figures S6 and S7 in SI), namely photochemically unreactive parallel conformers (***P*-*S*-1$_o$**) and reactive antiparallel conformers (***AP*-*S*-1$_o$**).[33,34,44] We utilized the B3LYP/6-31G* method to optimize the geometries and calculate the energy of ***P*-*S*-1$_o$** and ***AP*-*S*-1$_o$** (Table S2 in SI). The energy of ***P*-*S*-1$_o$** is smaller than ***AP*-*S*-1$_o$**, indicating ***P*-*S*-1$_o$** is preferred to self-assemble in an energy-efficient way. Furthermore, molecular modeling indicated that only ***P*-*S*-1$_o$** could self-assemble into well-ordered left-handed helixes (defined as

DOI: 10.1021/jacs.5b11580
J. Am. Chem. Soc. 2016, 138, 2219−2224

primary helixes, Figure 3g). Figure 3f shows the intermolecular hydrogen bonding between two neighboring chiral carboxylic groups. Then the primary helix is likely to relax into secondary helix (Figure 3h).[45] We proposed that the secondary helix is more favorable to accommodate the steric hindrance. Besides, the open form is structurally flexible enough to adapt to this torsion. The handedness of secondary helix is consistent with the primary one, while both the height and pitch of secondary helix are larger than the primary helix. The left-handed helixes observed from AFM images support our molecular modeling calculation. Nevertheless, the primary helical structures cannot be resolved with AFM. On the other hand, ***AP-S-1***$_o$ could not form primary left-handed helixes (Figure S8 in SI). Upon irradiation, the ring-closing reaction of ***AP-S-1***$_o$ to ***S-1***$_c$ resulted in an equilibrium shift from ***P-S-1***$_o$ to ***AP-S-1***$_o$, thus leading the disassembly of helixes. Fortunately, the irradiation of visible light recovers the initial equilibrium of helical self-assembly.

CONCLUSIONS

In summary, a rational design of hydrogen-bonded helical self-assembly based on photoswitchable DAEs can generate well-ordered left- and right-handed superhelixes that exhibit reversible morphological transformation upon light-stimuli. We achieved an unprecedented photoreversible modulation in morphology, fluorescence, and chirality amplification from molecular to supramolecular levels through helical self-assembly. The photoswitchable chiral amplification from helical self-assembly is easily accessible from small organic building blocks, serving as a great breakthrough to chiral communication between molecular and supramolecular chirality, similar to protein and DNA in natural systems.

ASSOCIATED CONTENT

Supporting Information

The Supporting Information is available free of charge on the ACS Publications website at DOI: 10.1021/jacs.5b11580.

More detailed experimental procedures, characterizations, supplementary optical spectra and figures (PDF)

AUTHOR INFORMATION

Corresponding Authors

*whzhu@ecust.edu.cn

*chi@uni-muenster.de

Author Contributions

§These authors contributed equally.

Notes

The authors declare no competing financial interest.

ACKNOWLEDGMENTS

This work was supported by National 973 Program (no. 2013CB733700), NSFC for Creative Research Groups (21421004) and Distinguished Young Scholars (21325625), NSFC/China, the Oriental Scholarship, Science and Technology Commission of Shanghai Municipality (15XD1501400), and the Fundamental Research Funds for the Central Universities (WJ1416005).

REFERENCES

(1) (a) Li, C.; Zhang, T.; Goldman, D. I. *Science* **2013**, *339*, 1408−1412. (b) Wolffs, M.; Delsuc, N.; Veldman, D.; Anh, N. V.; Williams, R. M.; Meskers, S. C. J.; Janssen, R. A. J.; Huc, I.; Schenning, A. *J. Am. Chem. Soc.* **2009**, *131*, 4819−4829.

(2) (a) Zhang, F.; Nangreave, J.; Liu, Y.; Yan, H. *J. Am. Chem. Soc.* **2014**, *136*, 11198−11211. (b) Dong, Y. C.; Yang, Z. Q.; Liu, D. S. *Acc. Chem. Res.* **2014**, *47*, 1853−1860.

(3) (a) Xu, J. F.; Chen, L. H.; Zhang, X. *Chem. - Eur. J.* **2015**, *21*, 11938−11946. (b) Palmer, L. C.; Stupp, S. I. *Acc. Chem. Res.* **2008**, *41*, 1674−1684. (c) Huang, F. H.; Anslyn, E. V. *Chem. Rev.* **2015**, *115*, 6999−7000.

(4) Kundu, P. K.; Samanta, D.; Leizrowice, R.; Margulis, B.; Zhao, H.; Börner, M.; Udayabhaskararao, T.; Manna, D.; Klajn, R. *Nat. Chem.* **2015**, *7*, 646−652.

(5) Wilner, O. I.; Orbach, R.; Henning, A.; Teller, C.; Yehezkeli, O.; Mertig, M.; Harries, D.; Willner, I. *Nat. Commun.* **2011**, *2*, 540−547.

(6) Luo, F.; Fan, C. B.; Luo, M. B.; Wu, X. L.; Zhu, Y.; Pu, S. Z.; Xu, W. Y.; Guo, G. C. *Angew. Chem., Int. Ed.* **2014**, *53*, 9298−9301.

(7) Yan, X. Z.; Cook, T. R.; Wang, P.; Huang, F. H.; Stang, P. J. *Nat. Chem.* **2015**, *7*, 342−348.

(8) Hill, D. J.; Mio, M. J.; Prince, R. B.; Hughes, T. S.; Moore, J. S. *Chem. Rev.* **2001**, *101*, 3893−4012.

(9) George, S. J.; de Bruijn, R.; Tomović, Ž.; Van Averbeke, B.; Beljonne, D.; Lazzaroni, R.; Schenning, A.; Meijer, E. W. *J. Am. Chem. Soc.* **2012**, *134*, 17789−17796.

(10) (a) Wu, J.; Fechtenkötter, A.; Gauss, J.; Watson, M. D.; Kastler, M.; Fechtenkötter, C.; Wagner, M.; Müllen, K. *J. Am. Chem. Soc.* **2004**, *126*, 11311−11321. (b) Ghosh, S.; Li, X. Q.; Stepanenko, V.; Würthner, F. *Chem. - Eur. J.* **2008**, *14*, 11343−11357.

(11) San Jose, B. A.; Ashibe, T.; Tada, N.; Yorozuya, S.; Akagi, K. *Adv. Funct. Mater.* **2014**, *24*, 6166−6171.

(12) Hoeben, F. J. M.; Jonkheijm, P.; Meijer, E. W.; Schenning, A. *Chem. Rev.* **2005**, *105*, 1491−1546.

(13) van Dijken, D. J.; Beierle, J. M.; Stuart, M. C. A.; Szymański, W.; Browne, W. R.; Feringa, B. L. *Angew. Chem., Int. Ed.* **2014**, *53*, 5073−5077.

(14) Palmans, A. R. A.; Meijer, E. W. *Angew. Chem., Int. Ed.* **2007**, *46*, 8948−8968.

(15) Duan, P. F.; Cao, H.; Zhang, L.; Liu, M. H. *Soft Matter* **2014**, *10*, 5428−5448.

(16) Li, Y. N.; Urbas, A.; Li, Q. *J. Am. Chem. Soc.* **2012**, *134*, 9573−9576.

(17) Wang, Y.; Li, Q. *Adv. Mater.* **2012**, *24*, 1926−1945.

(18) Kaiser, T. E.; Stepanenko, V.; Würthner, F. *J. Am. Chem. Soc.* **2009**, *131*, 6719−6732.

(19) Lu, X. Y.; Guo, Z. Q.; Sun, C. Y.; Tian, H.; Zhu, W. H. *J. Phys. Chem. B* **2011**, *115*, 10871−10876.

(20) Pantoş, G. D.; Pengo, P.; Sanders, J. K. M. *Angew. Chem., Int. Ed.* **2007**, *46*, 194−197.

(21) Shao, H.; Seifert, J.; Romano, N. C.; Gao, M.; Helmus, J. J.; Jaroniec, C. P.; Modarelli, D. A.; Parquette, J. R. *Angew. Chem., Int. Ed.* **2010**, *49*, 7688−7691.

(22) Irie, M.; Fukaminato, T.; Matsuda, K.; Kobatak, S. *Chem. Rev.* **2014**, *114*, 12174−12277.

(23) Yoon, J.; de Silva, A. P. *Angew. Chem., Int. Ed.* **2015**, *54*, 9754−9756.

(24) Chen, S. J.; Chen, L. J.; Yang, H. B.; Tian, H.; Zhu, W.-H. *J. Am. Chem. Soc.* **2012**, *134*, 13596−13599.

(25) Higashiguchi, K.; Taira, G.; Kitai, J.; Hirose, T.; Matsuda, K. *J. Am. Chem. Soc.* **2015**, *137*, 2722−2729.

(26) Meng, F.; Hervault, Y.; Shao, Q.; Hu, B.; Norel, L.; Rigaut, S.; Chen, X. *Nat. Commun.* **2014**, *5*, 3023−3032.

(27) Pace, T. C. S.; Müller, V.; Li, S.; Lincoln, P.; Andréasson, J. *Angew. Chem., Int. Ed.* **2013**, *52*, 4393−4396.

(28) Patra, A.; Métivier, R.; Brisset, F.; Nakatani, K. *Chem. Commun.* **2012**, *48*, 2489−2491.

(29) Mao, Y. Y.; Liu, K. Y.; Lv, G. L.; Wen, Y.; Zhu, X. J.; Lan, H. C.; Yi, T. *Chem. Commun.* **2015**, *51*, 6667−6670.

(30) Delbaere, S.; Berthet, J.; Shiozawa, T.; Yokoyama, Y. *J. Org. Chem.* **2012**, *77*, 1853−1859.

(31) Jiang, G.; Song, Y.; Guo, X.; Zhang, D.; Zhu, D. *Adv. Mater.* **2008**, *20*, 2888−2898.

DOI: 10.1021/jacs.5b11580
J. Am. Chem. Soc. 2016, 138, 2219−2224

(32) de Jong, J. J. D.; Lucas, L. N.; Kellogg, R. M.; van Esch, J. H.; Feringa, B. L. *Science* **2004**, *304*, 278−281.
(33) Yagai, S.; Iwai, K.; Yamauchi, M.; Karatsu, T.; Kitamura, A.; Uemura, S.; Morimoto, M.; Wang, H.; Würthner, F. *Angew. Chem., Int. Ed.* **2014**, *53*, 2602−2606.
(34) Yagai, S.; Iwai, K.; Karatsu, T.; Kitamura, A. *Angew. Chem., Int. Ed.* **2012**, *51*, 9679−9683.
(35) Li, M.; Ge, H. B.; Arrowsmith, R. L.; Mirabello, V.; Botchway, S. W.; Zhu, W.-H.; Pascu, S. I.; James, T. D. *Chem. Commun.* **2014**, *50*, 11806−11809.
(36) Lee, M. H.; Kim, J. Y.; Han, J. H.; Bhuniya, S.; Sessler, J. L.; Kang, C.; Kim, J. S. *J. Am. Chem. Soc.* **2012**, *134*, 12668−12674.
(37) (a) Berova, N.; Bari, L. D.; Pescitelli, G. *Chem. Soc. Rev.* **2007**, *36*, 914−931. (b) Chin, K. K.; Natarajan, A.; Gard, M. N.; Campos, L. M.; Shepherd, H.; Johansson, E.; Garcia-Garibay, M. A. *Chem. Commun.* **2007**, 4266−4268.
(38) Allenmark, S. *Chirality* **2003**, *15*, 409−422.
(39) Hirose, T.; Irie, M.; Matsuda, K. *Adv. Mater.* **2008**, *20*, 2137−2141.
(40) Kamer, P. C. J.; Cleij, M. C.; Nolte, R. J. M.; Harada, T.; Hezemans, A. M. F.; Drenth, W. *J. Am. Chem. Soc.* **1988**, *110*, 1581−1587.
(41) Nolte, R. J. M. *Chem. Soc. Rev.* **1994**, *23*, 11−19.
(42) Martin, R. B. *Chem. Rev.* **1996**, *96*, 3043−3064.
(43) Ponnuswamy, N.; Pantoş, G. D.; Smulders, M. M. J.; Sanders, J. K. M. *J. Am. Chem. Soc.* **2012**, *134*, 566−573.
(44) Li, W.; Jiao, C.; Li, X.; Xie, Y.; Nakatani, K.; Tian, H.; Zhu, W.-H. *Angew. Chem., Int. Ed.* **2014**, *53*, 4603−4607.
(45) Li, L.-S.; Jiang, H. Z.; Messmore, B. W.; Bull, S. R.; Stupp, S. I. *Angew. Chem., Int. Ed.* **2007**, *46*, 5873−5876.

DOI: 10.1021/jacs.5b11580
J. Am. Chem. Soc. 2016, 138, 2219−2224